# Structure of an RNA Hairpin from HRV-14

He Huang,*,‡ Andrei Alexandrov,‡ Xiaoying Chen,§ Thomas W. Barnes III,§ Hong Zhang,§ Kaushik Dutta,‡ and Steven M. Pascal*,‡

*Department of Biochemistry and Biophysics, University of Rochester Medical Center, Box 712, Rochester, New York 14642, and Department of Chemistry, University of Rochester, Rochester, New York 14627-0216*

*Received March 21, 2001; Revised Manuscript Received May 8, 2001*

ABSTRACT: The 5′ noncoding region of the picornaviral genome begins with a cloverleaf which is required for viral replication, due at least in part to an interaction with the viral RNA polymerase as part of a fusion with the predominant viral protease. The necessary region of the cloverleaf has previously been narrowed to a highly conserved stem−loop. The solution structure of a 14-nucleotide RNA hairpin, which is part of the conserved stem−loop from human rhinovirus isotype 14, is presented here. The secondary structure of the hairpin is identical to predictions: a five base pair stem is bounded by a triloop with sequence UAU. However, the fold of the triloop is novel, with stacking of the second loop base onto the closing base pair of the stem, and deviations from A form geometry are introduced into the stem regions bordering the triloop, particularly on the 3′ side. These deviations and the associated triloop structure could help to explain the distinct sequence conservation and mutational analysis data observed for the stem region of the hairpin, as compared to a second sequentially similar stem in the intact stem−loop.

Human rhinoviruses are members of the picornavirus family, which encompasses 230 or so isotypes including the hepatitis A virus, poliovirus, and other enteroviruses (*1*). Genetic information is carried as a single-stranded small (∼7000−8500 bases) RNA molecule. The viral genome is replicated directly by a viral-encoded RNA-dependent RNA polymerase (RDRP or 3D),[1] without an intermediate DNA step. The 5′-cloverleaf from the noncoding region of the viral genome [Figure 1(a)] is necessary for viral replication (*2*−*6*) although it is not capable of attracting the isolated 3D protein (RDRP). Instead, it interacts with the 3C protein, the protease which is responsible for most of the cleavage events that reduce the viral polyprotein to its individual constituents. During part of the viral life cycle, the 3C protease remains fused to the 3D polymerase, and thus recruitment of 3C also brings 3D to the 5′-cloverleaf. The region of the 5′-cloverleaf necessary to attract 3C or the 3CD fusion has been narrowed to a single stem−loop [27 nucleotides in HRV14, Figure 1(b)] (*7*, *8*). The possibility of blocking viral replication has made this interaction a target of considerable interest.

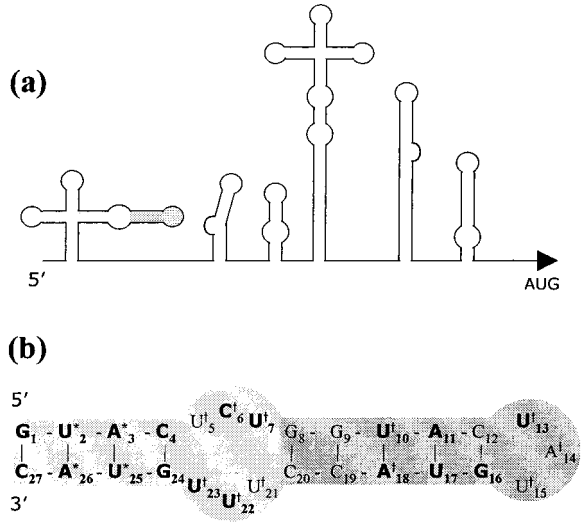


FIGURE 1: Schematic representation of the predicted secondary structure of the HRV-14 RNA 5′-NCR. (a) The entire 5′-NCR. Aside from the 5′-cloverleaf, most of the remainder of the 5′-NCR comprises the independent ribosomal entry site. (b) An expansion of the third hairpin loop from the 5′-cloverleaf (nucleotides 46−72), renumbered from 1 to 27. Conserved nucleotides are in boldface. Nucleotides which when mutated abrogate 3C binding are marked by an asterisk (*). Nucleotides which when mutated do not substantially interfere with 3C binding are marked by a dagger (†). See Discussion for further definition of mutants. The present study was performed using nucleotides 8−20 (darker shading) with an additional 3′-dangling A for stem stability ($A_{21}$).

* To whom correspondence should be addressed. Phone: 716-273-4832. Fax: 716-275-6007. Email: hehuang@mc.rochester.edu or pascal@oxbow.biophysics.rochester.edu.

‡ University of Rochester Medical Center.

§ University of Rochester.

[1] Abbreviations: 3C, protease 3C from picornavirus; 3D, protein 3D which is the RNA-dependent RNA polymerase from picornavirus; 3CD, fusion of 3C and 3D proteins; RDRP, RNA-dependent RNA polymerase; HRV14, human rhinovirus isotype 14; NCR, noncoding region; HPLC, high-performance liquid chromatography; NMR, nuclear magnetic resonance; fid, free induction decay; $T_1$, longitudinal relaxation time; $T_2$, transverse relaxation time; NOE, nuclear Overhauser effect; NOESY, nuclear Overhauser effect spectroscopy; DQF-COSY, double quantum filtered correlation spectroscopy; TOCSY, total correlation spectroscopy; HMQC, heteronuclear multiple quantum coherence; HETCOR, heteronuclear correlation; UV, ultraviolet; $\Delta G°_{37}$, change in free energy under standard conditions at 37 °C; $\Delta H°$, change in free energy under standard conditions; $\Delta S°$, change in entropy under standard conditions; $T_m$, melting temperature; $^3J_{HaHb}$, three-bond scalar coupling between proton a and proton b.

10.1021/bi010572b CCC: $20.00 
Published on Web 06/14/2001

A secondary structure prediction of this conserved stem−loop points out several interesting characteristics, including the presence of GUAC self-complimentary sequences in stem I and stem II, a U-rich 3 × 3 internal loop, and a 3-nucleotide UAU hairpin loop. Various double and multiple base substitutions (*8*), together with sequence conservation analysis, suggest that the most important determinants of 3C protease binding are carried in the stem region, in particular stem I [Figure 1(b)]. This is an intriguing finding for two reasons. First, RNA protein contacts are thought to occur mostly through single-stranded or distorted helical RNA regions [for a review, see (*9*)], and so the 3C/RNA complex could represent a novel RNA/protein binding motif. Second, stem I appears to be more critical for 3C binding, despite the fact that the base sequences of stem I and stem II are very similar. Distinctions could reflect differences in the three-dimensional structure or accessibility of the two stem regions. The presence of the UAU triloop is also of interest. To this point, the three-dimensional structure of an RNA triloop with a purine at the second position has not been reported. Since purines have a higher propensity to stack than pyrimidines (*10*), a novel triloop fold might be expected. The influence that this sort of triloop might have upon the stability and conformation of the adjoining stem region is also unknown.

In this study, we have determined the structure of a 14-nucleotide RNA hairpin representing the hairpin loop and the adjoining stem from stem−loop d of the 5′-cloverleaf of HRV14 [Figure 1(b), darker shading]. The predicted secondary structure holds: five Watson−Crick base pairs are detected in a largely A form geometry. The UAU triloop adopts a novel conformation, with the central adenosine base stacked upon the closing C·G base pair of the stem. The requirements of triloop formation also appear to have introduced deviation from A form geometry in the adjoining stem, particularly 3′ to the triloop. The triloop structure and stem distortions could help to explain the nonequivalence of stem I and stem II in 3C binding.

## MATERIALS AND METHODS

*RNA Preparation.* The oligoribonucleotide 5′-GGUAC-UAUGUACCA-3′ (referred to as 14mer, molecular mass = 4431.7 Da) was purchased from Dharmacon (Lafeyette, CO) after chemical synthesis, gel electrophoresis, and HPLC purification. The 2′-*o*-ester protection (*11*−*13*) was removed with 100 mM TEMED-acetate (tetramethylethylenediamine), pH 3.8, as described by the manufacturer. The oligomer was further purified with ethanol precipitation and gel filtration, and buffer-exchanged to 90 mM NaCl, 10 mM sodium phosphate, 0.1 mM EDTA, pH 7.0. For NMR studies, the oligomer concentration was brought to 1.5 mM, and $H_2O$ was replaced by either 100% $D_2O$ ($D_2O$ sample) or 10% $D_2O$/90% $H_2O$ ($H_2O$ sample).

*Thermodynamic Measurements.* Absorbance versus temperature was measured at 280 nm with a heating rate of 1.0 °C/min on a Gilford 250 spectrophotometer. The absorbance versus temperature profile was fit to a two-state model using the MeltWin 3.0 Program (*14*). Oligomer concentration was varied over a greater than 100-fold range from 3.4 to 370 $\mu$M.

*NMR Spectroscopy.* All NMR experiments were performed on a Varian INOVA 600 MHz spectrometer, processed with VNMR (Varian Inc.) or nmrPipe (*15*), and visualized and analyzed with NMRDraw (*15*), NMRview (*16*), and Felix (MSI Inc.). In general, spectra of nonexchangeable protons were recorded at 25 °C and exchangeable protons at 0 °C. One-dimensional spectra of nonexchangeable protons were obtained with the watergate solvent suppression scheme (*17*), while exchangeable protons were observed using a binomial 1331 solvent suppression pulse sequence (*18*). $^1$H $T_1$ relaxation rates were determined in $D_2O$ using the inversion−recovery method.

Most two-dimensional NMR spectra were acquired with a 100% $D_2O$ sample, and the residual HDO resonance was suppressed by low-power presaturation. The only exceptions were NOESY spectra, which were recorded both with the $D_2O$ and with the $H_2O$ samples. The $H_2O$ NOESY (*19*) was acquired with a 120 ms mixing time at 0 °C, and the $H_2O$ peak was suppressed by a combination of soft 90° pulses and z-gradient pulses during the mixing time, to observe broadened resonances (*20*). A total of 256 $t_1$ increments were acquired, with 4096 data points and 32 scans per fid, spectral widths of 12 500 Hz in each dimension, and a recycle time of 3 s. $D_2O$ NOESY spectra were acquired with mixing times of 50, 75, 100, 120, and 400 ms at 25 °C. Spectra were recorded with standard $(90°-t_1-90°-\text{mix}-90°-\text{acquire})_n$ pulse sequence with similar parameters as the $H_2O$ NOESY, except the spectral widths were reduced to 6000 Hz in each dimension. $D_2O$ NOESY spectra were also recorded at 0, 20, and 35 °C to assist in assignment of resonances and NOEs.

The DQF-COSY spectrum (*21*) was recorded at 25 °C, with the standard $(90°-t_1-90°-90°-\text{acquire})_n$ pulse sequence. A total of 512 $t_1$ increments were acquired, with 4096 data points and 64 scans per fid and a recycle time of 0.55 s. The spectrum was $^{31}$P broad-band-decoupled during $t_1$, and $^{31}$P Waltz-16 decoupled during acquisition. TOCSY spectra (*22*, *23*) with mixing times of 70 and 200 ms were recorded at 20 and 25 °C, using the standard $(90°-t_1-\text{MLEV}-\text{acquire})_n$ pulse sequence. A total of 400 $t_1$ increments were acquired, with 4096 data points and 16 transients per fid and a recycle time of 3.3 or 4.3 s. Spectral widths were 6000 Hz in each dimension for the DQF-COSY and TOCSY spectra. A natural-abundance $^1$H,$^{13}$C-HMQC spectrum (*24*−*27*) was acquired with spectral widths of 5000 and 10 560 Hz in the proton and carbon dimensions, respectively. A total of 60 increments were acquired, with 2048 data points and 512 scans per fid and a recycle time of 3 s. A $^1$H−$^{31}$P HETCOR spectrum (*28*) was acquired with spectral widths of 5000 Hz in $^1$H and 800 Hz in $^{31}$P. A typical data set consisted of 80 $t_1$ increments with 2048 points and 256 transients per fid and a 2.2−2.5 s recycle time.

All two-dimensional data sets were apodized with a 27° shifted sine bell squared function in both dimensions. For coupling constant extraction, DQF-COSY and HETCOR spectra were reprocessed with an unshifted sine bell squared function, and the method of Kim and Prestegard (*29*) was employed.

*NMR-Derived Structural Constraints.* NOE-based estimates of the distance between nonexchangeable protons were derived from NOESY cross-peak volumes at mixing times of 50, 75, and 100 ms using an isolated spin approximation. Cross-peak volumes were integrated using Felix and buildup rates compared to H5−H6 (2.45 Å) cross-peaks and scaled

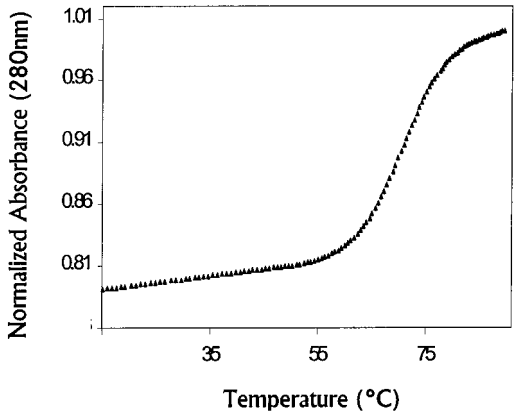


FIGURE 2: Plot of normalized absorbance (280 nm) vs temperature. The sample was 20 $\mu$M RNA 14mer in 90 mM NaCl, 10 mM sodium phosphate, 0.1 mM EDTA, pH 7.0. $T_m$ is 71.7 °C, and varies by less than 1% from this value over a concentration range of 3.4−370 $\mu$M.

by $1/r^6$ where $r$ represents the distance between the two protons. After distances were derived in this manner, the potential well minima and maxima were set to 90% and 130% of this distance, and the upper bound was increased to 140% or 150% in cases of overlap, up to a maximum of 6 Å. The absence of a sequential NOE between U15(H6) and A14(H2′) was used to derive a lower bound constraint of 5.0 Å. NOEs involving exchangeable protons were interpreted conservatively as distance constraints with lower and upper bounds of 1.8 and 5.0 Å, respectively.

*Structure Determination.* Structural modeling, calculations, visualization, and analysis were performed using Insight II 2000 and Discover (MSI, Inc.) running on an SGI workstation. The AMBER force field was used for all calculations with full-scale van der Waals and electrostatic interactions. A 12 Å cutoff was used for nonbonding interactions. Force constants for distance and dihedral restraints were set to 25 kcal/Å and 25 kcal/(mol·rad$^2$), respectively. Four hundred cycles of restrained energy minimization were followed by 5 ps of restrained molecular dynamics starting with random velocities and ramping down from 1000 to 298 K. After another 80 000 cycles of restrained energy minimization, 10 000 cycles of nonrestrained energy minimization were performed to provide an energy-minimized structure.

## RESULTS

*Thermodynamics of Hairpin Formation.* Secondary structure prediction suggests that the 14mer forms a single stem−loop with a three-member hairpin turn. The predicted stability is $\Delta G°_{37} = -5.0$ kcal/mol via a nearest-neighbor free energy calculation using mfold version 3.0 (*30, 31*). The UV absorbance as a function of temperature for the 14mer is shown in Figure 2. A characteristic melting profile is observed, with a $T_m$ of 71 °C. The concentration independence of this curve (data not shown) indicates that the 14mer is unimolecular in aqueous solution. The melting profile also confirms that the 14mer is conformationally stable over the temperature range used for NMR study (0−35 °C). The experimentally derived thermodynamic parameters for hairpin formation are $\Delta H° = -53.0 \pm 1.9$ kcal/mol, $\Delta S° = -153.98 \pm 5.4$ eu, and $\Delta G°_{37} = -5.3 \pm 0.2$ kcal/mol.

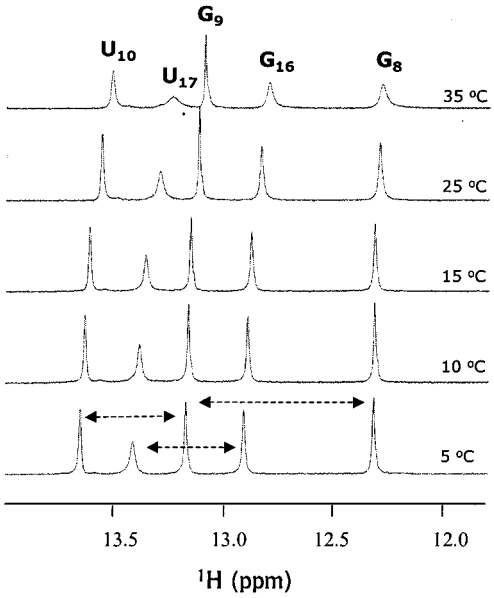


FIGURE 3: Imino region of 1D $^1$H NMR at five temperatures. Peaks between which intrachain NOEs were observed are connected by dashed arrows above the 5 °C spectrum. Broadening of the $G_8$, $G_{16}$, and $U_{17}$ peaks at higher temperatures indicates either exchange with solvent or conformational exchange on a millisecond to microsecond time scale.

*Exchangeable Proton Resonance Assignment and Interpretation.* The imino proton regions of one-dimensional $^1$H NMR spectra of the oligomer at different temperatures are shown in Figure 3. There are seven imino protons in the 14mer, five of which produce observable resonances. Assigning the two missing peaks to U13 and U15 of the loop (later confirmed), the pattern of sequential imino−imino NOEs in the $H_2O$ NOESY spectrum at 0 °C (denoted above the 5 °C spectrum in Figure 3) divides the peaks into two groups: G8/G9/U10 and G16/G17. G9 was identified by virtue of its NOEs to both G8 and G10. G8 and G16 were initially differentiated from U10 and U17 on the basis of chemical shift. These assignments were confirmed, and amino and H2 protons were assigned by analysis of NOEs from cytosine amino protons to the base-paired guanidine imino protons, and from uridine imino protons to the base-paired adenine amino and H2 protons. The G8 amino protons were easily observed and assigned due to the presence of the 3′-dangling A, which increases the stability of the terminal base pair (*32*).

Most resonances in Figure 3 shift by less than 0.1 ppm from 5 to 35 °C, a characteristic which is shared by the nonexchangeable resonances (data not shown). Together with the UV melting curve (Figure 2), this suggests that there is little conformational variation over this temperature range. The broadening with temperature observed for the G8 and G16 imino protons is consistent with positioning at the stem terminal and closing base pair, whereas G9 and U10 are less broadened due to internal positioning. Somewhat surprisingly, the intensity of the U17 imino peak is approximately half of the intensity of the remaining imino peaks, even at 5 °C. This could indicate either partial accessibility to solvent and subsequent exchange with $H_2O$ or a dynamic transition on the millisecond to microsecond scale. The absence of observed peaks for the imino protons of U13 and U15 suggests a lack of stable hydrogen bonding for these loop nucleotides.

Table 1: $^{1}$H, $^{13}$C, and $^{31}$P Chemical Shift Assignments[a] (ppm)

| residue | imino H1/3 | amino H2/4/6 | H8/6 (C8/6) | H5/2 (C5/2) | H1′ (C1′) | H2′ | H3′ | H4′ | H5′/5″[b] | $^{31}$P |
|---|---|---|---|---|---|---|---|---|---|---|
| G8 | 12.28 | 6.25/8.08 | 8.17 (138.6) | − | 5.97 (93.4) | 4.97 | 4.62 | 4.50 | 4.16/4.01 | − |
| G9 | 13.14 | 6.09/NA[c] | 7.48 (136.7) | − | 5.85 (93.3) | 4.54 | 4.63 | 4.18 | NA | −0.21 |
| U10 | 13.63 | −[d] | 7.78 (141.4) | 5.19 (103.1) | 5.55 (93.7) | 4.52 | 4.58 | 4.50 | 4.16 | −0.68 |
| A11 | − | 6.33/8.29 | 8.10 (141.9) | 7.21 (83.9) | 6.04 (93.1) | 4.38 | 4.70 | 4.52 | 4.16/4.08[e] | −0.33 |
| C12 | − | 6.71/7.88 | 7.39 (140.4) | 5.03 (97.7) | 5.59 (92.3) | 4.39 | 4.67 | 4.40 | 4.07 | −0.51 |
| U13 | NA | − | 7.90 (144.0) | 5.90 (105.4) | 5.94 (90.3) | 4.44 | 4.58 | 4.37 | 4.15/4.07 | 0.25 |
| A14 | − | NA | 8.10 (130.5) | 8.08 (85.3) | 5.68 (91.0) | 4.44 | 4.57 | 4.11 | 4.17/4.01 | −0.57 |
| U15 | NA | − | 7.81 (144.0) | 5.85 (105.8) | 6.01 (89.6) | 4.33 | 4.76 | 4.39 | 3.92/3.80 | 0.71 |
| G16 | 12.89 | 6.32/8.27 | 8.23 (138.4) | − | 5.77 (94.1) | 4.87 | 4.74 | 4.28 | 3.92/3.80 | 0.16 |
| U17 | 13.40 | − | 7.92 (143.8) | 5.30 (103.7) | 5.76 (88.5) | 4.65 | 4.59 | 4.49 | NA | 0.51 |
| A18 | − | 6.48/8.09 | 8.28 (139.9) | 7.11 (83.5) | 6.10 (92.9) | 4.49 | 4.78 | 4.56 | 4.39/4.25 | −0.33 |
| C19 | − | 6.98/8.37 | 7.61 (140.8) | 5.26 (97.1) | 5.40 (93.5) | 4.22 | 4.39 | 4.50 | 4.08 | −0.67 |
| C20 | − | 6.97/8.23 | 7.62 (140.8) | 5.42 (98.0) | 5.48 (94.0) | 4.42 | 4.45 | 4.38 | 4.21/4.08 | −0.58 |
| A21 | − | NA | 8.04 (140.2) | 7.37 (84.5) | 6.00 (92.0) | 4.07 | 4.32 | 4.27 | 3.80 | −0.24 |

[a] Exchangeable $^{1}$H resonances were assigned at 0 °C, other resonances at 25 °C. For referencing of $^{1}$H shifts, the $H_2O$ resonance of a sample not containing RNA was measured at 5.02 and 4.79 ppm vs TSP at 0 and 25 °C, respectively. The $H_2O$ resonances of the RNA samples at 0 and 25 °C were then referenced to these values. $^{13}$C chemical shifts were referenced via indirect calibration (*52, 53*), and $^{31}$P was referenced to 85% $H_3PO_4$. [b] H5′ and H5″ resonances were not stereoassigned. H5′ is listed as downfield by convention only. [c] NA: not assigned due to overlap or exchange with solvent. [d] (−): there is no such atom for this residue. [e] Underline: chemical shift could not be measured accurately due to overlap.

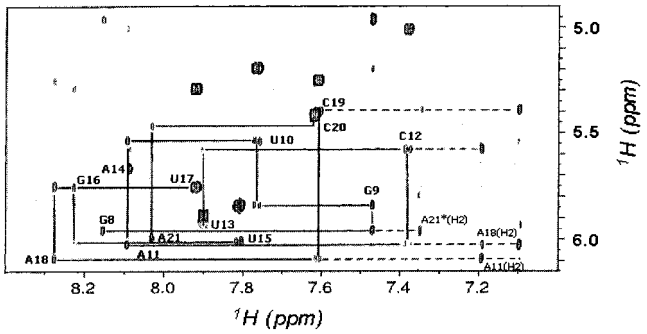


FIGURE 4: Portion of the NOESY spectrum demonstrating sequential resonance assignment strategy. Peaks representing intranucleotide H8/H6−H1′ NOEs are labeled. Solid lines connect these peaks to the sequential H8/H6($i$+1)−H1′($i$) NOE peaks. H1′−H2(adenosine) NOE peaks are connected to the above NOE peaks by dashed lines, and labeled in a smaller font.

*Nonexchangeable Proton Resonance Assignment.* The base to H1′ and H5 region of a 400 ms NOESY spectrum is shown in Figure 4. Assignments of nonexchangeable protons were made using standard procedures, and are reported in Table 1. To overcome spectral overlap, some chemical shift assignments were confirmed by comparison with NOESY spectra at various temperatures. DQF-COSY and TOCSY spectra were also used. The H2 protons of A11, A18, and A21 were distinguished from other base protons by their characteristically long $T_1$ relaxation times and NOEs to base-paired uridine imino protons as discussed above. Further confirmation of the adenine H2 assignments was obtained from a natural-abundance $^{1}$H,$^{13}$C-HMQC spectrum. Adenine C2 nuclei resonate far downfield and are well separated from other $^{13}$C resonances. NOEs to the A14 H2 proton were not observed in the NOESY spectrum. However, by elimination of the other H2 proton resonances in the $^{1}$H,$^{13}$C-HMQC spectrum, the A14 H2 chemical shift could be assigned. The large dispersion of carbon chemical shift also helped to complete and confirm assignments of H1′ protons, other sugar protons, and H5 protons of cytosine and uridine.

*$^{31}$P Resonance Assignment and Interpretation.* The $^{1}$H-$^{31}$P HETCOR experiment enabled assignment of the phosphorus resonances (Figure 5). The strongest cross-peaks are

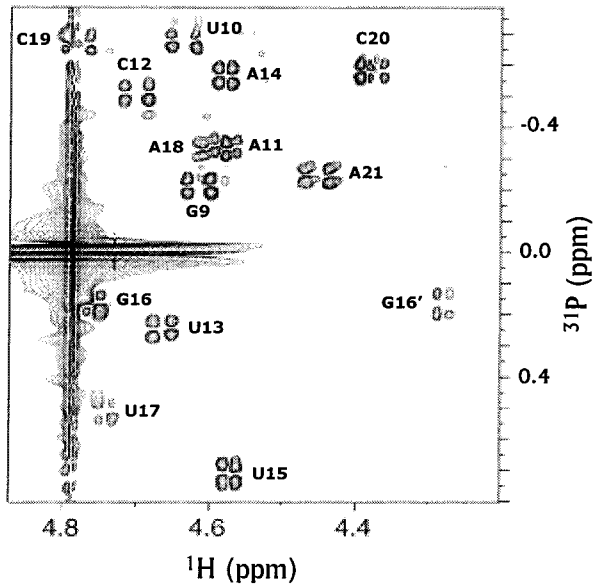


FIGURE 5: Portion of a $^{1}$H,$^{31}$P-HETCOR spectrum. H3′($i$−1)−P($i$) cross-peaks are labeled. The H4′($G_{16}$)−P($G_{16}$) at the far right is labeled as G16′.

the sequential H3′($i$−1)−P($i$) correlations, which are labeled in the figure. Most of the phosphorus resonances are observed between −0.8 and 0.0 ppm, which is typical of base-paired stem regions (*33*). The $^{31}$P nuclei of U13, U15, G16, and U17 resonate between 0.0 and +0.8 ppm, indicating a backbone conformation in this region which is not consistent with A form geometry. The values of the U13, U15, and G16 chemical shifts are not surprising due to their presence in the 3-nucleotide turn, while the extreme shift of U15 is evidence for a strong element of irregularity at this position. However, the position of the U17 phosphorus resonance adds further support to the possibility of a local distortion of the helical stem. The inclusion of the A14 $^{31}$P resonance within the −0.8 to 0.0 ppm range indicates that the backbone between U13 and A14 is oriented differently than in other regions of the loop. $^{31}$P chemical shifts can be influenced by a number of factors, including backbone dihedral angles, solvent accessibility, hydrogen bonding, and other electro-

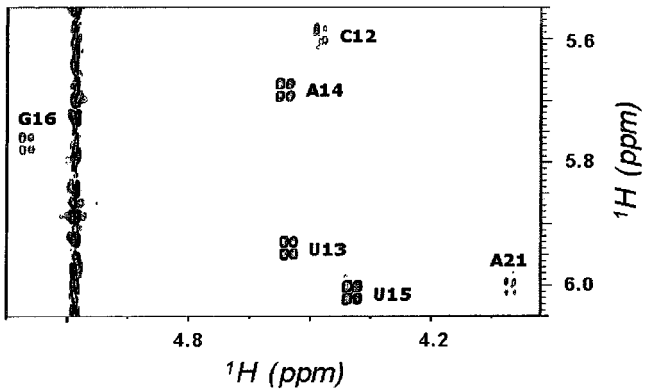


FIGURE 6: H1′−H2′ region of the DQF-COSY spectrum. Visible cross-peaks indicate relatively large $^3J_{H1'H2'}$ values, suggesting at least partial C2′-*endo* character.

static interactions. Direct interpretation of the chemical shifts is therefore difficult, beyond the identification of unusual regions and comparison with similar chemical shifts from similar sequences.

*Sugar Pucker*. In the DQF-COSY spectrum (Figure 6), the H1′−H2′ multiplet patterns of the three nucleotides in the hairpin loop (U13, A14, U15) exhibit doublet patterns with $^3J_{H1'H2'} = 6-8$ Hz. These large couplings indicate a predominantly C2′-*endo* sugar conformation (S type), which was used to derive a constraint with a lower bound of 90° and an upper bound of 165° for the $\delta$ dihedral angle (C5′−C4′−C3′−O3′). The G16(H1′) resonance is also doublet with $^3J_{H1'H2'} = 5.4$ Hz, and the A21 and C12 cross-peaks have couplings of approximately 2.5 Hz. These intermediate values suggest an equilibrium between C3′-*endo* and C2′-*endo* conformations, and so $\delta$ was loosely restrained to between 70° and 165°. The absence of peaks from the rest of the base-paired stem is likely due to very small couplings and is consistent with a C3′-*endo* (N type) pucker, and thus the remaining $\delta$ dihedral angles were restrained to between 70° and 110°.

*Glycosidic Torsion Angles.* In the 100 ms NOESY spectrum collected at 25 °C (data not shown, refer to Figure 4), nearly all of the base to H1′ cross-peaks are far weaker than the cytosine and uridine intranucleotide H5−H6 cross-peaks, indicating that the glycosidic torsion angles are in anti conformations. Note that the peak labeled U13 overlaps with the U13(H5−H6) NOE, and the area labeled by C19 and C20 contains four NOEs [C19(H6−H1′), C20(H6)−C19(H1′), C20(H6−H1′), C20(H6−H5)]. These peaks are resolved at lower temperature, and anti glycosidic torsion angles are confirmed. However, the U17 peak overlaps with the U17(H6)−G16(H1′) NOE. These two NOEs are partially resolved at 0 °C, revealing that the U17(H6)−G16(H1′) NOE is approximately half the intensity of the U17(H6−H5) NOE, while the U17(H6−H1′) is considerably weaker. Therefore, the U17 glycosidic bond is also anti, but a backbone irregularity may exist between G16 and U17. Dihedral angle restraints were not constructed from glycosidic bond information.

*Secondary Structure.* Five Watson−Crick base pairs were detected by virtue of the following: (a) five observable imino peaks; (b) the chemical shift values of these peaks; (c) five cross-strand imino−amino NOEs (G8−C20, G9−C19, U10−A18, U17−A11, G16−C12). In addition, U10−A18 and U17−A11 imino−H2 NOEs were observed. Hence, Watson−Crick hydrogen bond restraints were applied to the five base pairs of the stem (*34*). The NOE walk traced out in Figure 4 is typical of the connectivities in an A form helix, with the exception of the missing connectivities from U13 through U15. The A21(H2)−G8(H1′) NOE is consistent with stacking of the A21 base onto the G8·C20 base pair. The A11(H2)−A18(H1′) and A18(H2)−A11(H1′) NOEs are further confirmation of A form geometry. However, A form geometry in the form of backbone dihedral angle constraints was imposed only on three base pairs (G8·C20, G9·C19, U10·A18) due to detected irregularities in the remaining portion of the stem (see below).

*Hairpin Loop NOEs.* The weak U13(H5)−C12(H2′) and U13(H6)−C12(H1′) NOEs (estimated distances of 5.5 and 4.0 Å, respectively) are the only interresidue NOEs to U13, suggesting that the U13 base is extruded from the interior of the loop. The intermediate U15(H1′)−G16(H8) NOE (∼3.5 Å) involving the U15 sugar is the only internucleotide NOE observed to U15, suggesting that the U15 base is also extruded. Together with the observation of A14(H8)−C12(H1′) and A14(H4′)−G16(H1′) NOEs (approximately 4.3 and 4.6 Å, respectively), the data suggest that extrusion of the U13 and U15 bases allows the A14 base to stack onto the C12·G16 base pair.

*Evidence of Stem Distortion.* Despite the presence of five base pairs, there exists considerable evidence of departure from ideal A form geometry. The $^3J_{H1'H2'}$ values for G16 and C12 of 5.4 and 2.5 Hz, respectively (see Figure 6), indicate at least partial population of a C2′-*endo* sugar conformation, particularly for G16. The $^{31}$P chemical shift of U17 (attached to the 5′-end of the U17 ribose) is anomalously downfield-shifted (Figure 5). As discussed above, the strength of the U17(H6)−G16(H1′) NOE suggests a backbone irregularity may exist between G16 and U17. Furthermore, only two of the four typical A form NOEs were observed between G16 sugar protons and U17 base protons. Together, these data suggest helical irregularities in the two base pairs closest to the hairpin loop, particularly near the G16 sugar and U17 base. No such irregularities were found associated with the three terminal base pairs.

## DISCUSSION

*Analysis of Calculated Structures.* Structures were calculated using the energy minimization and molecular dynamics protocol described under Materials and Methods. NOE and dihedral angle constraints were not violated past a threshold value of 0.1 Å or 1°, respectively, in any of the calculated structures or the minimized average structure. Figure 7(a) shows the superposition of the 15 calculated structures, and Figure 7(b) shows the energy-minimized structure. The RMSD per nucleotide is given in Table 2.

Five Watson−Crick base pairs are present, connected by a three-nucleotide loop, as is consistent with the input constraints. The positions of the terminal three base pairs of the stem, together with A21, are defined to an average RMSD of 0.27 Å, whereas the loop and the closing two base pairs (C12·G16, A11·U17) are less well-defined. This is in part due to the A form constraints applied to the well-defined base pairs, but also reflects the larger number of inter-

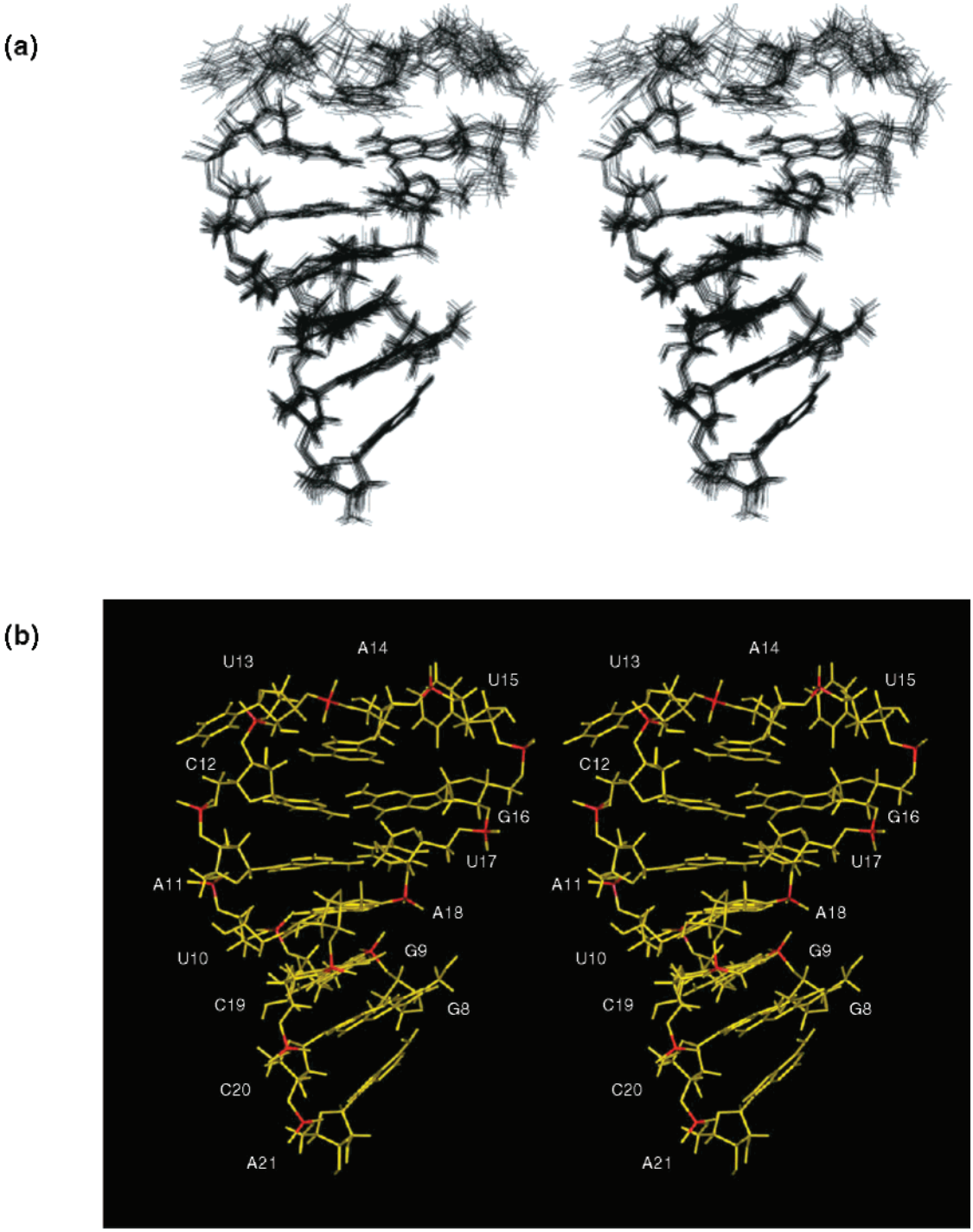


FIGURE 7: Stereoview of (a) a superposition of the 15 calculated structures. (b) The minimized average structure. Phosphate atoms are drawn in red.

nucleotide NOEs involving the well-defined nucleotides. A total of 17 internucleotide NOEs were observed to G16 or U17, compared with 25 to G9 or U10 from the opposite end of the GUAC sequence. This asymmetry results largely from covering of the G9·C19 base pair with the G8·C20 base pair, while C12·G16 directly borders the hairpin turn. So while the GUAC sequence repeats, the structure is not symmetric. As anticipated, the 3′-dangling A21 base stacks onto the G8·C20 base pair. This results in sharpening of the imino proton resonance of G8 (which might otherwise be unobservable), and is predicted to cause an increase in the stability of the hairpin stem.

Extrusion of the U13 and U15 bases allows the A14 base to stack upon the C12·G16 base pair. The most variable positioning is for the U15 base, to which there were no internucleotide NOEs detected. While the conformation of the backbone allows the U15 base to approach the major groove as if it might partially stack onto G16, it swings up and away, allowing A14 to stack instead. The U15 base approaches the A14 base in a perpendicular manner in most of the calculated structures, but little evidence exists to identify hydrogen bonds or other interactions which may secure it in place. The U13 base is also extruded, but with a very different geometry. The backbone configuration results

Table 2: Number of Restraints and Average RMSD (Å) between the Final and the Average Structures

| base | NOE intra/inter | dihedral restraints | RMSD[a] | RMSD[b] |
|---|---|---|---|---|
| G8 | 11/8 | 4 | 0.27 | 0.24 |
| G9 | 6/13 | 6 | 0.28 | 0.25 |
| U10 | 4/12 | 6 | 0.25 | 0.23 |
| A11 | 7/14 | 2 | 0.34 | 0.29 |
| C12 | 6/11 | 1 | 0.50 | 0.51 |
| **U13[f]** | **11/2** | **1** | **0.96** | **1.05** |
| **A14** | **7/2** | **1** | **0.92** | **0.98** |
| **U15** | **6/1** | **1** | **1.61** | **1.72** |
| G16 | 9/7 | 1 | 0.55 | 0.52 |
| U17 | 6/10 | 1 | 0.50 | 0.45 |
| A18 | 6/15 | 5 | 0.29 | 0.26 |
| C19 | 7/12 | 6 | 0.30 | 0.29 |
| C20 | 4/10 | 4 | 0.21 | 0.19 |
| A21 | 7/5 | 1 | 0.30 | 0.29 |
| total[c] | 73/61 | 37 | 0.34 | 0.32 |
| total[d] | 24/5 | 3 | 1.16 | 1.25 |
| total | 97/61[e] | 40 | 0.52 | 0.52 |

[a] All atoms were superimposed. [b] Base-paired stem residues (8−12, 16−20) were superimposed. [c] Subtotal for stem bases (8−12, 16−21). [d] Subtotal for loop bases (13−15). [e] All internucleotide NOEs involved at least one stem nucleotide. [f] The boldfaced residues represent the hairpin loop residues. Dihedral restraints for A form geometry are included in the totals. Hydrogen bond distances for WC base pairs and the U15(H6) to A14(H2′) non-NOE are not included.

in the U13 base projecting directly away from the loop interior, and it is constrained to approach the edge of the minor groove by weak U13(H5)−C12(H2′) and U13(H6)−C12(H1′) NOEs. A potential U13(O5′)−C12(HO2′) hydrogen bond could contribute to the stability of this position, which leaves the U13 base relatively isolated and solvent-exposed. While the orientation of the A14 base is restricted to a plane which is nearly parallel to the C12·G16 base pair plane, its exact position within that plane is not precisely defined by the A14(H8)−C12(H1′) and A14(H4′)−G16(H1′) NOEs. Its position spreads out in this plane, in concert with variation in the U13 and U15 conformations, resulting in a RMSD for A14 which is similar to the U13 value.

The backbone dihedral angles are plotted in Figure 8. The boxes within each graph denote the dihedral constraints used for the calculation. Recall that $^3J_{H1'H2'}$ values were used to constrain all 14 $\delta$ dihedral angles. G8 through A11 and U17 through C20 were constrained to a C3′-*endo* conformation, and in fact converge to 80° much more tightly than the 70−110° restraints require. U13, A14, and U15 $\delta$ angles were constrained to 90−165° (C2′-*endo*), and 43 of the 45 triloop $\delta$ angles converged to angles greater than 120°. The closing base pair (C12·G16) and A21 were constrained only to 70−165° (C2′-*endo* or C3′-*endo*), yet each converges toward 80° (C3′-*endo*). Additional dihedral constraints arose from enforcement of A form geometry from G8($\gamma$) through A11-($\alpha$) and from A18($\beta$) through C20($\gamma$), effectively covering the three terminal base pairs (G8·C20, G9·C19, U10·A18). However, the A21 angles, the regions of C20 not constrained ($\epsilon$,$\zeta$), and the A11 angles also converge to A form values. Note that the phosphate group 5′ to G8 is absent, and so G8 $\alpha$ and $\beta$ angles are nonexistent. The dihedral angles of the loop residues do not converge to A form geometry. The dihedral angles in this region are extremely variable from structure to structure, particularly at U15. The remaining bases are C12·G16 and U17 (partner of A11). C12 diverges from A form only slightly, with the most marked excursions seen in $\alpha$ and $\gamma$, and slight shifts in the envelope of values for $\epsilon$ and $\zeta$. The G16 and U17 $\epsilon$ and $\zeta$ values are A form-like, while the $\gamma$ values cluster around a non A-like 180°. The $\alpha$ and $\beta$ patterns are different for the two residues. G16 populates two rotamers for $\alpha$ (∼−80°, +60°) and $\beta$(−90°, +60°). The values of these two angles are always of opposite sign (compensatory torsions). The U17 $\beta$ values are A-like with the exception of one structure, but the $\alpha$ angles form two clusters, one A-like (∼−80°) and the other in a region which is disallowed for A form (∼180°). An overall picture emerges of a predominantly A-like stem from G8−C12 [except C12($\gamma$)] and A18−A21, with a three-nucleotide turn from U13−U15, and a distorted stem backbone, with possibly two conformers, at G16 and U17. The main distortions involve G16 $\alpha$,$\beta$,$\gamma$ and U17 $\alpha$,$\gamma$. It should be noted that no inconsistencies were found between the A form and Watson−Crick constraints and the NOEs or $\delta$ dihedral angle constraints. Note also that the computed structures match NMR data which were not used to generate restraints. The unusual $^{31}$P shifts for G16 and U17 match the irregularities in the backbone, and the $^{31}$P shifts for U13 and U15 are consistent with extrusion of these bases. All glycosidic bonds are anti as predicted, except U15 which appears somewhat intermediate, reflecting again the total absence of internucleotide NOEs to the U15 base.

*Comparison with Previously Described RNA Triloops.* The central triloop base, A14, stacks onto the closing base pair of the stem, while the two U bases are extruded. In examining the structures of four RNA triloops discussed in the literature, this appears to be a novel loop conformation. Although the first and third positions in three of the triloops were also occupied by U, the central position was occupied by either U (*35*) or C (*36, 37*). Although stacking of the central base onto the first loop nucleotide sugar was seen, weak NOEs have been interpreted in terms of possible partial stacking (*35*), and in one case the first loop base was observed extending down into the minor groove along the helical axis, approaching the stem base pairs from the edge (*37*), in none of these cases was there strong evidence for stacking of the loop bases onto the stem bases. More recently, the structure of a triloop with sequence AUA was determined (*38*), and here the third loop base was seen to stack onto the closing base pair, suggesting a preference for purine bases, or at least A, to stack in this manner. In this case, the first loop base (also A) resides in a position where a minor rearrangement might allow stacking onto the closing base pair, but this location is already occupied by the third loop base, perhaps forcing the first base to swing up and out toward the major groove. A structure of a triloop containing guanosine has yet to appear.

Each of the three UAU triloop sugars adopt primarily C2′-*endo* conformations, with average $\delta$ values above 120° (Figure 8). Interpreting the $^3J_{H1'H2'}$ coupling constants via the formula % C3′-*endo* = 114.9 − 14.5($J_{H1'H2'}$) (*39*), the loop base coupling constants of 6.5, 6.1, and 7.7 Hz suggest 79, 74, and 97% C2′-*endo* conformation, respectively. This is consistent with the triloop $^3J_{H1'H2'}$ constants from the NMR structures discussed above (*35, 36, 38*), where the smallest coupling was 5.8 Hz (69% C2′-*endo*), and the average coupling is approximately 7.3 Hz (91% C2′-*endo*). It appears that predominantly C2′-*endo* conformations may be highly

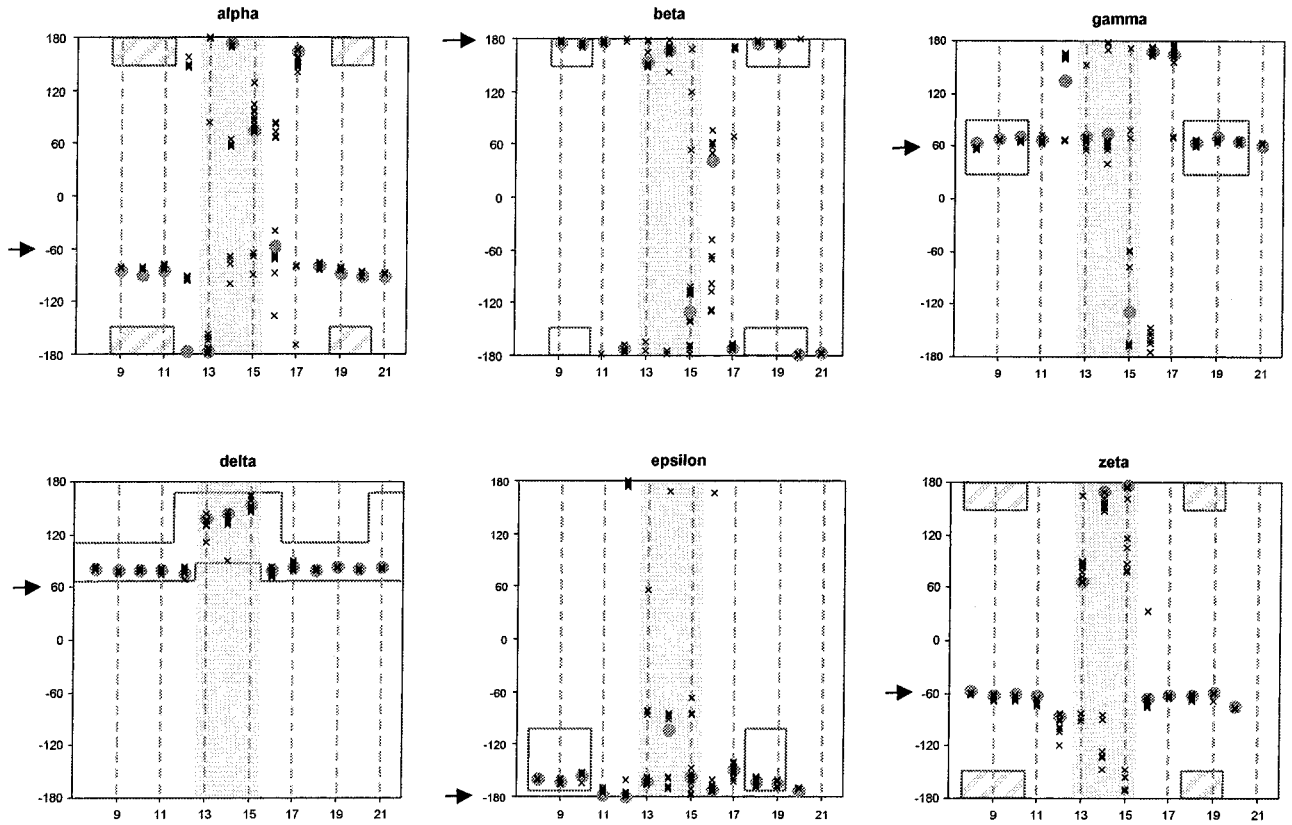


FIGURE 8: Backbone dihedral angle plots for the 15 calculated structures (x) and the minimized average structure (gray circles). The shaded rectangle in the center of each plot delineates the loop residues. Nonshaded box regions represent dihedral angle restraints. Diagonally shaded boxes (α and ζ) represent regions disallowed by dihedral angle restraints. The arrow to the left of each plot indicates the approximate value typical of A form geometry.

preferred in order to accommodate triloop structures, and, pertinently, to span the distance between the 5′ and 3′ stem backbones with just three nucleotides: switching from C3′-*endo* to C2′-*endo* can increase the intrachain P(*i*)−P(*i*+1) distance from 5.8 to 7.0 Å (*10*). In the case of the present study, two of the sequential phosphate distances in the triloop exceed 7.0 Å. However, in the crystal structure discussed above (*37*), the second and third loop sugars occupy predominantly C3′-*endo* conformations, and the first loop sugar is in an intermediate state. Returning to the present study, the only glycosidic bond in the UAU triloop to show partial syn character was U15, the third loop base, and this may result simply from lack of data (no internucleotide NOEs to this base were observed). However, the two other triloop structures with well-determined loop base orientations have third loop bases in a syn (*38*) or in an intermediate (*37*) conformation. In addition, the first loop base glycosidic bond is also an intermediate state in the crystal structure. One possible explanation for the disparities between the crystal and NMR structures is the nature of the closing base pair. In the crystal structure, the triloop is closed by an A·U pair, which has been shown to introduce a free energy penalty of +0.6 kcal/mol when compared with closure by other Watson−Crick pairs (*40*), whereas triloops in the NMR studies are closed by U·G (*36*) or C·G (*35, 38*).

*Stem Distortions Near the Loop*. The evidence of stem distortion in the regions bordering the UAU triloop, particularly at the closing two 3′ bases, was discussed above. One notable feature is the presence of trans γ angles (see Figure 8) at the +1, +2, and −1 positions (first and second nucleotides 3′, and first nucleotide 5′ to the triloop). Stem distortions near the loop were also present in each of the triloop structures discussed above, and appear to be more common or more pronounced on the 3′ side in the NMR structures, including trans γ at the +1 (*35*) and +2 (*35, 38*) positions. The crystal structure shows a similar pattern of distortion, although somewhat more equally distributed to the stem regions 5′ and 3′ to the triloop, including trans γ angles at the −1 and +2 positions. It is interesting to note that in each of these triloops, any detected trans γ angles were found at the ±1 pyrimidine or the +2 purine nucleotides. Trans γ angles in stem nucleotides 3′ to tetraloops have also been reported (e.g. *41*−*43*).

*Stem*−*Loop Structure and RNA Replication.* Referring to Figure 1(b), the following mutations (*8*) of stem−loop d from HRV do not interfere with the interaction between 3C and the 5′-cloverleaf in vitro: (a) mutation of the UAU triloop to AUA or GGG; (b) mutation of the stem II U10·A18 base pair to C·G; (c) reflection of the internal loop sequence, to place UUU on the 5′ strand and UCU on the 3′ strand; (d) "closing" of the internal loop with the multiple substitution U21A/U22G/U23A. The following mutations abrogate or severely impair 3C binding: (e) mutation of the U2·A26 and U25·A3 base pairs to C·G; (f) a multiple mutation which eradicates base-pairing from G8 through C20, resulting in a single large loop extending from U5 through U23 (base pairing may be present within the loop); (g) a global antisense mutation of the stem, which effectively converts the UAU triloop to AUA (previously shown to be benign above) and the internal loop from U-rich to A-rich. In addition, the analogous cloverleaf from poliovirus was able to bind HRV14 3C protease (*8*). To convert from the HRV to the

poliovirus stem−loop d sequence, the following changes are necessary: (h) mutation of the internal loop (U7C and U21C); (i) mutation of the UAU triloop to a UGCG tetraloop; (j) a stem II alteration which converts the closing base pair to a reverse wobble (C12U). These results, together with the higher sequence conservation of stem I vs stem II among human rhinoviruses [Figure 1(b)], suggest that the GUAC self-complimentary sequences in each stem play nonequivalent roles in 3C binding. This distinction is likely due to differences in structure or accessibility.

The presence of the extra G8·C20 pair in stem II could play a role in distinguishing the two stems. In addition to this pair, the 27mer contains four other G·C base pairs, each of which is part of a GUAC sequence (two pairs in stem I and two in stem II). Despite this homogeneity, the nearest-neighbor environments of these four base pairs differ. The G9·C19 base pair is likely the most stable, and adopts canonical A form geometry in this study, in large part due to the presence of the G8·C20 base pair. The G1·C27 base pair is at the stem terminus, and should be relatively unstable. In the context of the intact cloverleaf, the environment of this pair is certainly altered, bordering an AG mismatch pair in HRV 14, and bordering a two nucleotide bulge and an additional three base pair stem region in the poliovirus cloverleaf. However, since these additional nucleotides are not necessary for 3C binding in vitro, it can be assumed that increased stability of the G1·C27 base pair is not necessary for 3C binding, and indeed instability may be required. The two remaining G·C pairs, G16·C12 and G24·C4, would at first appear to be in similar environments, each bordering a loop with a UU first mismatch. However, as we have shown, the triloop structure results in stacking of the A14 base onto G16·C12 and extrusion of the U13 and U15 bases. This arrangement would be very difficult for the internal loop to mimic, as it contains no purines. The U5 and U23 bases may even hydrogen bond across the helical axis. Indeed, since closing the internal loop has a minimal effect on 3C binding [mutation (d) above], a disrupted G24·C4 base pair is apparently not necessary for 3C binding, and a stable G24·C4 base pair may be required.

Since distortion of the two closing base pairs was seen in the RNA 14mer, nonequivalence of the A11·U17 base pair with the other A·U pairs in the 27mer may also contribute to the distinction between the two stems. This distortion is likely due to the presence of the UAU triloop. While tetraloop structures are common in other stem−loop d sequences (see above), it is worthwhile to note that nearly all of the mutational analysis of HRV-14 discussed above was conducted in the presence of a triloop. It remains a possibility that substitution of a tetraloop which causes less stem distortion may remove some of the distinction between stems I and II. However, this would not explain the stronger sequence conservation of stem I. In this context, it is important to note three observations: (i) as previously mentioned, stem distortion has been seen in areas bordering RNA tetraloops. Thus, stem distortion reaching to the second closing pair, or certainly the closing pair, may remain in stem II in the presence of a tetraloop. (ii) In an alignment of HRV and poliovirus stem−loop d regions containing tetraloops, there is a strong tendency for an U·G pair to close the stem, as opposed to the C·G closing pair of the HRV 14 triloop. It is possible that some instability or irregularity of stem II is necessary for proper functioning of the stem−loop, and that this can be accomplished through introduction either of a triloop or of a reverse wobble closing base pair. (iii) Sequence conservation data may reflect not only the requirements for 3C binding, but other as yet unidentified functions. (iv) However, the in vitro mutational analysis does suggest that the 3C protease recognizes primarily the stem I region. This is an intriguing concept, particularly in light of mutation (d) above, which closes off the internal loop and presumably results in a stable nondistorted A form stem I helix (in fact, stem I and stem II would merge). Most RNA−protein interactions would be expected to occur at or near single-stranded regions or distorted helical regions, for instance near bulge loops (*44*−*49*), although examples have been seen of binding to the major groove of a mostly undistorted A form helix near a hairpin turn (*50*, *51*). The fact that mutation of the U·A pairs in stem I to C·G pairs [mutation (e) above] abrogates 3C binding suggests either that 3C is capable of recognizing the nature of the bases within an essentially undistorted A form helix, or that 3C causes distortion or partial unfolding of the helix. It is possible that the increase in stability brought on by the addition of two hydrogen bonds [mutation (e)] affects the ability of 3C to distort or unfold the helix, but it is also possible that the U·A base pairs are required for specific recognition once the distortion occurs. A more complete understanding of this interaction awaits a structural determination of the 3C protease/RNA complex.

## ACKNOWLEDGMENT

We gratefully acknowledge the contributions of Thomas Krugh, Douglas Turner, Susan Schroder, and Scott Kennedy.

## REFERENCES

1. Pringle, C. R. (1996) *Arch. Virol. 141*, 2251−2256.
2. Trono, D., Andino, R., and Baltimore, D. (1988) *J. Virol. 62*, 2291−2299.
3. Andino, R., Rieckhof, G. E., and Baltimore, D. (1990) *Cell 63*, 369−380.
4. Andino, R., Rieckhof, G. E., Trono, D., and Baltimore, D. (1990) *J. Virol. 64*, 607−612.
5. Andino, R., Rieckhof, G. E., Achacoso, P. L., and Baltimore, D. (1993) *EMBO J. 12*, 3587−3598.
6. Rohll, J. B., Percy, N., Ley, R., Evans, D. J., Almond, J. W., and Barclay, W. S. (1994) *J. Virol. 68*, 4384−4391.
7. Leong, L. E., Walker, P. A., and Porter, A. G. (1993) *J. Biol. Chem. 268*, 25735−25739.
8. Walker, P. K., Leong, L. E. C., and Porter, A. G. (1995) *J. Biol. Chem. 270*, 14510−14516.
9. Hard, T. (1999) *Q. Rev. Biophys. 32*, 57−98.
10. Saenger, W. (1990) *Principles of Nucleic Acid Structure*, Springer-Verlag, New York.
11. Anderson, A. C., Scaringe, S. A., Earp, B. E., and Frederick, C. A. (1996) *RNA 2*, 110−117.
12. Scaringe, S. A., Wincott, F. E., and Caruthers, M. H. (1998) *J. Am. Chem. Soc. 120*, 11820−11821.
13. Scaringe, S. A., Francklyn, C., and Usman, N. (1990) *Nucleic Acids Res. 18*, 5433−5441.
14. McDowell, J. A., and Turner, D. H. (1996) *Biochemistry 35*, 14077−14089.
15. Delaglio, F., Grzesiek, S., Vuister, G. W., Zhu, G., Pfeifer, J., and Bax, A. (1995) *J. Biomol. NMR 6*, 277−293.
16. Johnson, B. A., and Blevins, R. A. (1994) *J. Biomol. NMR 4*, 603−614.
17. Piotto, M., Saudek, V., and Sklenar, V. (1992) *J. Biomol. NMR 2*, 661−665.
18. Hore, P. J. (1983) *J. Magn. Reson. 55*, 283−300.

19. Kumar, A., Wagner, G., Ernst, R., and Wüthrich, K. (1981) *J. Am. Chem. Soc. 103*, 3654−3658.
20. Chen, X., McDowell, J., Turner, D. H., and Krugh, T. R. (2000) *Biophys. J. 78*, 1836Pos.
21. Rance, M., Sorensen, O. W., Bodenhausen, G., Wagner, G., Ernst, R. R., and Wüthrich, K. (1983) *Biochem. Biophys. Res. Commun. 117*, 479−485.
22. Braunschweiler, L., and Ernst, R. R. (1983) *J. Magn. Reson. 53*, 521−528.
23. Bax, A. D., and Davis, D. G. (1985) *J. Magn. Reson. 65*, 355−360.
24. Bodenhausen, G., and Ruben, D. J. (1980) *Chem. Phys. Lett. 69*, 185−189.
25. Bax, A., Griffey, R. H., and Hawkins, B. L. (1983) *J. Magn. Reson. 55*, 301−315.
26. Cavanagh, J., and Keeler, J. (1988) *J. Magn. Reson. 77*, 356−362.
27. Bax, A., Ikura, M., Kay, L. E., Torchia, D. A., and Tschudin, R. (1990) *J. Magn. Reson. 86*, 304−318.
28. Sklenar, V., Miyashiro, H., Zon, G., Miles, H. T., and Bax, A. (1986) *FEBS Lett. 208*, 94−98.
29. Kim, Y. M., and Prestegard, J. H. (1989) *J. Magn. Reson. 84*, 9−13.
30. Mathews, D. H., Sabina, J., Zuker, M., and Turner, D. H. (1999) *J. Mol. Biol. 288*, 911−940.
31. Zuker, M., Mathews, D. H., and Turner, D. H. (1999) in *RNA Biochemistry and Biotechnology* (Clark, J. B. B. F. C., Ed.) pp 11−43, Kluwer Academic Publishers, Dordrecht, The Netherlands.
32. Burkard, M. E., Kierzek, R., and Turner, D. H. (1999) *J. Mol. Biol. 290*, 967−982.
33. Legault, P., and Pardi, A. (1994) *J. Magn. Reson., Ser. B 103*, 82−86.
34. Pappalardo, L., Kerwood, D. J., Pelczer, I., and Borer, P. N. (1998) *J. Mol. Biol. 282*, 801−818.
35. Davis, P. W., Thurmes, W., and Tinoco, I., Jr. (1993) *Nucleic Acids Res. 21*, 537−545.
36. Puglisi, J. D., Wyatt, J. R., and Tinoco, I., Jr. (1990) *Biochemistry 29*, 4215−4226.
37. Cate, J. H., Gooding, A. R., Podell, E., Zhou, K. H., Golden, B. L., Kundrot, C. E., Cech, T. R., and Doudna, J. A. (1996) *Science 273*, 1678−1685.
38. Kim, C. H., Kao, C. C., and Tinoco, I., Jr. (2000) *Nat. Struct. Biol. 7*, 415−423.
39. van den Hoogen, F. (1988) Ph.D. Dissertation, University of Leidin.
40. Serra, M. J., Barnes, T. W., Betschart, K., Gutierrez, M. J., Sprouse, K. J., Riley, C. K., Stewart, L., and Temel, R. E. (1997) *Biochemistry 36*, 4844−4851.
41. Varani, G., Cheong, C., and Tinoco, I., Jr. (1991) *Biochemistry 30*, 3280−3289.
42. Jucker, F. M., and Pardi, A. (1995) *Biochemistry 34*, 14416−14427.
43. Schmitz, U., James, T. L., Lukavsky, P., and Walter, P. (1999) *Nat. Struct. Biol. 6*, 634−638.
44. Weeks, K. M., and Crothers, D. M. (1991) *Cell 66*, 577−588.
45. Weeks, K. M., and Crothers, D. M. (1993) *Science 261*, 1574−1577.
46. Puglisi, J. D., Chen, L., Blanchard, S., and Frankel, A. D. (1995) *Science 270*, 1200−1203.
47. Ye, X., Kumar, R. A., and Patel, D. J. (1995) *Chem. Biol. 2*, 827−840.
48. Ye, X. M., Gorin, A., Ellington, A. D., and Patel, D. J. (1996) *Nat. Struct. Biol. 3*, 1026−1033.
49. Battiste, J. L., Mao, H. Y., Rao, N. S., Tan, R. Y., Muhandiram, D. R., Kay, L. E., Frankel, A. D., and Williamson, J. R. (1996) *Science 273*, 1547−1551.
50. Cai, Z., Gorin, A., Frederick, R., Ye, X., Hu, W., Majumdar, A., Kettani, A., and Patel, D. J. (1998) *Nat. Struct. Biol. 5*, 203−212.
51. Legault, P., Li, J., Mogridge, J., Kay, L. E., and Greenblatt, J. (1998) *Cell 93*, 289−299.
52. Live, D. H., Davis, D. G., Agosta, W. C., and Cowburn, D. (1984) *J. Am. Chem. Soc. 106*, 1939−1941.
53. Bax, A., and Subramanian, S. (1986) *J. Magn. Reson. 67*, 565−569.

BI010572B